ELECTROSTATIC MODELING OF ION PORES

Energy Barriers and Electric Field Profiles

PETER C. JORDAN
Department of Chemistry, Brandeis University, Waltham, Massachusetts 02254

ABSTRACT This paper presents calculations of the image potential for an ion in an aqueous pore through lipid membrane and the electric field produced in such a pore when a transmembrane potential is applied. The method used is one introduced by Levitt (1978, *Biophys. J.* 22:209), who solved an equivalent problem, in which a surface charge density is placed at the dielectric boundary. It is shown that there are singularities in this surface charge density if the model system has sharp corners. Numerically accurate calculations require exact treatment of these singularities. The major result of this paper is the development of a projection method that explicitly accounts for this behavior. It is shown how this technique can be used to compute, both reliably and efficiently, the electrical potential within a model pore in response to any electrical source. As the length of a channel with fixed radius is increased, the peak in the image potential approaches that of an infinitely long channel more rapidly than previously believed. When a transmembrane potential is applied the electric field within a pore is constant over most of its length. Unless the channel is much longer than its radius, the field extends well into the aqueous domain. For sufficiently dissimilar dielectrics the calculated values for the peak in the image potential and for the field well within the pore can be summarized by simple empirical expressions that are accurate to within 5%.

INTRODUCTION

It is axiomatic that electrostatic interactions provide a significant energy barrier to the transport of ions across lipid membranes. Were it not for the presence of specialized molecules such as carriers or pores, the energy required to affect such translocations would be enormous. Parsegian (1969, 1975) considered the reduction in the barrier height in cases for which the pore length is very much greater than its radius. Levitt (1978) formulated an approach that permits treatment of pores of finite length. As demonstrated by Jordan (1981), barrier estimates based upon calculation of the image potential for structureless pores yield energies that are too high, even if dielectric shielding by the pore-forming molecule is taken into consideration. The test system, gramicidin A, has a nondiffusional energy barrier for passage of monovalent cations no greater than $\sim 6\ kT$. The total barrier for passage through a featureless channel with gramicidin A's gross physical structure is $\gtrsim 10\ kT$ so that it was suggested (Jordan, 1981) that the residual reduction in the translocation energy might be accounted for if the interaction with dipolar carbonyl groups (Urry, 1971) lining the channel were considered.

Carrying out such a calculation requires modification of the basic method introduced by Levitt (1978). Since the purpose of electrostatic calculations is to permit assessment of which physical and electrical features substantially influence the pore conductance, it is clear that whatever method is used the numerical results must be quite accurate. Small errors in the calculated energy barrier, because they are exponentiated, can lead to seriously inaccurate conductance estimates. In attempting to extend Levitt's (1978) treatment of the energies of ions in pores it became clear that even though the idea is correct, the numerical results obtained are very sensitive to the method used to solve the equations. This turns out to be especially serious when calculating the energy profile of an ion in a long, narrow pore, and when considering the electric field produced when a potential difference is applied to a membrane containing a pore.

If one wishes to retain model simplicity by portraying a "pore" as a right circular cylinder piercing a "membrane" slab, the equations describing this problem turn out to have singularities related to the fact that the model system has sharp edges. Although these singularities can be eliminated by constructing more realistic models in which all sharp corners are rounded off,[1] the basic equations become more complicated and require more computer time for solution. This paper exposes the nature of the "corner" singularities, develops a solution method that explicitly accounts for such behavior, and demonstrates how this method can be used to compute the electric potential within a pore in response to any electrical source. The method is applied to two problems: the image potential of an ion in a pore and the electric

[1] P. C. Jordan, unpublished calculations.

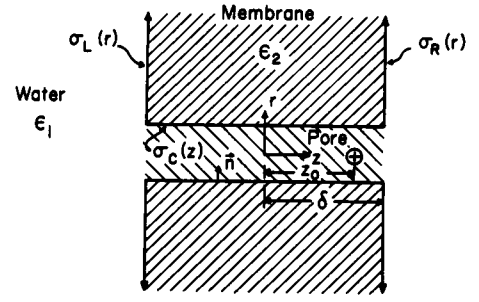

FIGURE 1 Cross-section of a cylindrical pore piercing a membrane slab of dielectric constant ϵ_2. The pore interior and the water are presumed to have the same dielectric constant ϵ_1. Distances are scaled in terms of a unit pore radius. A point source of strength q is located at z_0. The membrane thickness is 2δ. The σ are surface charge densities in the replacement system and $\vec{n}$ is the normal pointing outward from region 2.

field produced when a transmembrane potential is applied. The results clearly indicate the importance of treating the singularities exactly.

THEORY

Integral Equations for the Replacement Surface Charge Densities

The simplest model for describing an ion channel is shown in Fig. 1. An ion of charge q on the pore axis induces surface charges at the electrical phase boundaries. As shown by Levitt (1978), the electric potential can be calculated by solving a replacement problem in which the system is described as a uniform dielectric with a fictitious surface charge density situated along the phase boundaries. This charge density is chosen to recreate the electric-field discontinuity in the real system.

Using dimensionless coordinates (distance in units of pore radius a_0, potential in units of $q/\epsilon_1 a_0$, and surface charge density in units of q/a_0^2) the substitute electrical problem is

$$\sigma(\vec{r}) = g\vec{n} \cdot [\widetilde{\nabla\varphi}(\vec{r})] \qquad 2\pi g = (\epsilon_1 - \epsilon_2)/(\epsilon_1 + \epsilon_2) \tag{1}$$

$$\varphi(\vec{r}) = 1/|\vec{r} - z_0\vec{k}| + \int dS\, \sigma(\vec{r}')/|\vec{r} - \vec{r}'|. \tag{2}$$

Combining Eqs. 1 and 2 yields an integral equation for the surface charge density $\sigma(\vec{r})$; dS is an element of area on the phase boundary; and $\widetilde{\nabla\varphi}(\vec{r})$ is that portion of the replacement electric field that arises from all charges except those in the immediate vicinity of r. The ion is located at a point z_0 on the axis; the membrane width is 2δ. In Eq. 2 the ion is treated as a point source, an approximation that is known (Jordan, 1981) to negligibly influence the polarization energy.

Computational economy is achieved if channel symmetry is exploited and the symmetric and antisymmetric contributions to σ are treated separately. In this way the calculations only involve half the phase boundary. Defining

$$Y_1^{\pm}(r) = \pi[\sigma_R(r) \pm \sigma_L(r)],\ Y_2^{\pm}(z) = \pi[\sigma_C(z) \pm \sigma_C(-z)] \tag{3}$$

where σ_R, σ_L, and σ_C are surface charge densities along the membrane's right-hand side, its left-hand side, and the pore wall, respectively; one finds after substantial algebra,

$$Y_i^{+}(t_i) = g\{F_i^{+}(t_i) + \int_1^{\infty} d\rho\rho\, Q_{i1}^{+}(t_i, \rho) Y_1^{+}(\rho) + \int_0^{\delta} d\zeta\, Q_{i2}^{+}(t_i, \zeta) Y_2^{+}(\zeta)\} \tag{4}$$

where $t_1 = r$ and $t_2 = z$. The equations for $Y_i^{-}(t_i)$ are analogous. The kernels, Q_{ij}, are

$$Q_{11}^{\pm}(r, \rho) = \pm K_1(2\delta, r, \rho) \tag{5a}$$

$$Q_{12}^{\pm}(r, \zeta) = K_1(\delta - \zeta, r, 1) \pm K_1(\delta + \zeta, r, 1) \tag{5b}$$

$$Q_{21}^{\pm}(z, \rho) = K_2(z - \delta, 1, \rho) \pm K_2(z + \delta, 1, \rho) \tag{5c}$$

$$Q_{22}^{\pm}(z, \zeta) = K_2(z - \zeta, 1, 1) \pm K_2(2\delta - z - \zeta, 1, 1) \tag{5d}$$

with

$$K_1(a, b, c) = -\frac{4aE(\alpha)}{ST^2},$$

$$K_2(a, b, c) = \frac{2}{bS}\left\{K(\alpha) - \left[1 + \frac{2b(c-b)}{T^2}\right]E(\alpha)\right\} \tag{6a}$$

$$S = \{a^2 + (b + c)^2\}^{1/2},\ T = \{a^2 + (b - c)^2\}^{1/2},$$

$$\cos\alpha = T/S, \tag{6b}$$

where K and E are complete elliptic integrals of the first and second kind. The inhomogeneous terms in Eq. 4 are

$$F_1^{\pm}(r) = \pi[V_1(r, \delta - z_0) \pm V_1(r, \delta + z_0] \tag{7a}$$

$$F_2^{\pm}(z) = \pi[V_2(1, z - z_0) \pm V_2(1, z + z_0)] \tag{7b}$$

with

$$V_1(a, b) = -b/R^3,\ V_2(a, b) = a/R^3,\ R = \{a^2 + b^2\}^{1/2}. \tag{8}$$

Although Eq. 4 appears to be straightforward, it isn't. As is well known in the theory of elasticity, where similar equations arise (Erdogan and Gupta, 1972), the functions Y_i are singular as $r \to 1$ or $z \to \delta$: in other words, at the sharp edge where the pore cylinder pierces the membrane slab. This is not surprising since the surface charge densities establish the electric field discontinuity along the phase boundary. For the geometry of Fig. 1 and any other system that incorporates sharp edges into the model, one poses a question that is analogous to asking for the electric field at the tip of a lightning rod. While Y_i and σ have singularities, the electric potential $\varphi(\vec{r})$, given by Eq. 2, does not. Thus this approach to the calculation of $\varphi(\vec{r})$ remains valid; however care must be taken so that the results of numerical calculations are reliable.

There are two obvious ways to avoid the problem created by these singularities. One is to recognize that model geometries that introduce sharp corners are unrealistic. By rounding off the corner at the pore mouth and thereby modifying the channel shape, the singularities can be eliminated. Although a physically reasonable procedure, this has the disadvantage of adding a third charge-density function to the set Y_i, which increases the computational complexity of the problem. The compensation is that this procedure permits direct investigation of some effects that modifying channel shape has upon channel conductance (unpublished calculation).[1]

The other approach, which will be developed here, is to characterize the singularity and treat it exactly. In this way no additional function need be added to the set, Y_i. This method is especially useful if the ion-pore-membrane-water system is to be described by models involving more than two dielectric phases. More realistic treatments of ion channels need such elaboration (Jordan, 1981). Even with simple pore geometries, solving these problems requires increasing the number of charge density functions Y_i, thereby complicating the calculations. Altering the pore geometry to circumvent the singularities could prohibitively augment the necessary numerical work.

Singularity Analysis

The charge density functions Y_i are singular because the kernels Q_{ij} are ill-defined at sharp corners. In terms of new variables

$$x_1 = r - 1, x_2 = \delta - z, \xi_1 = \rho - 1, \xi_2 = \delta - \zeta \qquad (9)$$

both Q_{12} and Q_{21} contain terms with the functional form $-2\xi/(x^2 + \xi^2)$ when x and ξ approach zero. This quantity is either 0 or ∞ depending upon whether ξ or x is set equal to zero first; other limiting procedures permit any intermediate value to be obtained. Near the corner the dominant term in Eq. 4, for both symmetric and antisymmetric contributions to $\sigma(\vec{r})$, is

$$Y_1(x) = \int_0^1 \frac{-2g\xi d\xi}{x^2 + \xi^2} Y_2(\xi), \quad Y_2(x) = \int_0^1 \frac{-2g\xi d\xi}{x^2 + \xi^2} Y_1(\xi). \qquad (10)$$

In treating the singularity, the upper limit in each integral is arbitrary; for convenience it is chosen to be 1. It is clear from Eq. 10 that neither Y_i can approach a constant nonzero value as $x_i \to 0$. If Y_2 did, then integration shows that $Y_1 \propto \ln x$; this, when integrated, implies that $Y_2 \propto (\ln x)^2$. Repeating this procedure demonstrates that the Y_i can be represented as infinite power series in $\ln x$ as $x \to 0$. A more convenient representation, which is obviously consistent with Eq. 10, recognizes that the singularity in Y_i can be expressed in the form $x^{-\mu}$ as $x \to 0$. Similar singularities occur in physical problems; they are especially common in the study of the response of materials to elastic stress (Erdogan and Gupta, 1972). As will be made clear, $\mu < 0.335$, no matter what the values of ϵ_1 and ϵ_2, so that such a singularity has no physically unreasonable consequences. The induced electric potential (the image potential) found by substituting from Eq. 3 into the integral of Eq. 2 is finite everywhere.

In Appendix A expressions for Y_i, valid as $x \to 0$, are found. They can be written in a matrix formalism

$$\vec{\mathbf{Y}}(x) = \Omega(x) \cdot \vec{\mathbf{b}} \qquad \Omega(x) = \begin{pmatrix} C(x) & S(x) \\ S(x) & C(x) \end{pmatrix} \qquad (11a)$$

$$C(x) = [x^{\mu} + x^{-\mu}]/2 \quad S(x) = [x^{\mu} - x^{-\mu}]/2, \qquad (11b)$$

where μ is given by Eq. A5. The value of μ, and thus the strength of the singularity, only depends upon the parameter g, which from Eq. 1 is simply a measure of the dielectric dissimilarity of the two phases. It varies from zero, when $\mu = 0$ and there are no singularities, to $1/2\pi$, when μ takes on its maximum value 0.3345118. The vector $\vec{\mathbf{b}}$, as yet undetermined, depends upon the other parameters of the system, in this case the position of the ion z_0, the half-width of the membrane δ, and whether the symmetric or antisymmetric functions $\vec{\mathbf{Y}}(x)$ are being calculated.

In addition to establishing μ, the analysis of Appendix A shows that Eq. 11 is exact as $x \to 0$. Whatever correction there is to $\vec{\mathbf{Y}}(x)$, it approaches zero more rapidly than x^{μ}. A formulation valid for all x is

$$\vec{\mathbf{Y}}(x) = \vec{\mathbf{w}}(x) + \Omega(x) \cdot \vec{\mathbf{b}}, \qquad x < 1 \qquad (12a)$$

$$\vec{\mathbf{Y}}(x) = \vec{\mathbf{w}}(x), \qquad x > 1 \qquad (12b)$$

where $\vec{\mathbf{w}}(x)$ is $0(x^{1-\mu})$ as $x \to 0$. Since μ is always less than 0.3345118, the correction is clearly smaller than x^{μ} in the small x domain. The representation used requires that $\vec{\mathbf{w}}$ be discontinuous at $x = 1$; this is done so that no computational problems arise at large x. For large values of x, $\vec{\mathbf{w}} \to 0$. The discontinuity in $\vec{\mathbf{w}}$ is

$$\vec{\mathbf{w}}(1_+) - \vec{\mathbf{w}}(1_-) = \vec{\mathbf{b}} \qquad (13)$$

Both $\vec{\mathbf{b}}$ and $\vec{\mathbf{w}}(x)$ can now be determined by substituting Eq. 12 into Eq. 4 and demanding that $\vec{\mathbf{w}}(x) \to 0$ as $x \to 0$. This program is sketched in Appendix B and yields the fundamental results of our analysis,

$$\vec{\mathbf{w}}(x) = g[\mathbf{F}(x) + \langle \mathbf{Q}(x, \xi) \cdot \vec{\mathbf{w}}(\xi) \rangle + \mathbf{U}(x) \cdot \vec{\mathbf{b}}] \qquad (14a)$$

$$\vec{\mathbf{b}} = -\mathbf{U}^{-1}(0) \cdot [\mathbf{F}(0) + \langle \mathbf{Q}(0, \xi) \cdot \vec{\mathbf{w}}(\xi) \rangle] \qquad (14b)$$

where the auxiliary matrix $\mathbf{U}(x)$ is given by Eqs. B1 and B4. The notation $\langle\ \rangle$ indicates integration over the variables ξ_1 or ξ_2: $0 \le \xi_1 \le \infty, 0 \le \xi_2 \le \delta$. Direct substitution of Eq. 14b into 14a demonstrates that $w(x) \to 0$ as $x \to 0$. In this form there are no residual singularities; Eqs. 14a and b can be solved rapidly and reliably by straightforward iteration numerical methods, among them successive approximations. A possible initial approximation is $\vec{\mathbf{b}}_0 = -\mathbf{U}(0)^{-1} \cdot \vec{\mathbf{F}}(0)$ and $\vec{\mathbf{w}}_0(x) = g[\vec{\mathbf{F}}(x) + \mathbf{U}(x) \cdot \vec{\mathbf{b}}_0]$. Other initial values are also possible; whatever is done must ensure that the basic constraint $\vec{\mathbf{w}}(x) \to 0$ as $x \to 0$ is satisfied at each iteration level.

Averaging Functional Corrections

As mentioned by Levitt (1978) a particularly good way to solve integral equations arising in electrostatics is to use the method of averaging functional corrections (Luchka, 1965). This is also true for the problem posed by Eqs. 14a, b. However the procedure must be modified in a significant way if the small x constraint on $\vec{\mathbf{w}}(x)$ is to be incorporated. The essentials are outlined in Appendix C.

Polarization Energy

The solution to Eq. 4 is determined by Eqs. 12 and 14; the symmetric and antisymmetric contributions to the surface charge density functions σ are treated separately. The polarization energy for an ion at z_0 on the axis is then proportional to the integral term in Eq. 2; the result is

$$E = \frac{q^2}{2\epsilon_1 a_0} 2\pi \left\{ \int_1^{R^*+1} dr r[\sigma_L(r) V(z_0 + \delta, r) + \sigma_R(r) V(z_0 - \delta, r)] + \int_{-\delta}^{\delta} dz \sigma_c(z) V(z_0 - z, 1) \right\} \qquad (15a)$$

$$V(a, b) = 1/[a^2 + b^2]^{1/2} \qquad (15b)$$

where R^* is the range of the r integration. The reason for truncation is discussed in Appendix C.

This method of solution leads to rapidly convergent, computationally reliable results. All peculiarities introduced by the sharp corners are handled exactly. The technique can be readily modified to treat a variety of electrostatic problems involving the same basic geometry.

Profile of an Applied Potential

The analysis just presented must be altered slightly to calculate the profile due to an applied potential. Following the arguments of Levitt (1978) the replacement surface charge-density functions are again defined by Eqs. 3–6. The analogue to Eq. 7 is

$$F_1^- = \epsilon_2 V_0 / 2\epsilon_1 \delta, F_2^- = 0, \quad F_i^+ = 0 \quad i = 1, 2 \qquad (16)$$

where V_0 is the applied potential difference. This formulation presumes that the solutions bathing the membrane are essentially nonconducting (zero ionic strength). Given this limitation it is readily seen that, for large r,

$$Y_i^-(r) \to Y_\infty = \alpha \epsilon_2 V_0 / 2\epsilon_1 \delta, \alpha = 2\pi g / (1 - 2\pi g). \qquad (17)$$

$r \to \infty$.

Defining

$$Y_1^-(r) = Y_\infty[1 + y_1(r)], \quad Y_2^-(z) = Y_\infty y_2(z) \tag{18}$$

where $y_1(r) \to 0$ as $r \to \infty$, the basic integral equations become

$$\vec{y}(x) = g\{\vec{f}(x) + \langle \mathbf{Q}^-(x,\xi) \cdot \vec{y}(\xi)\rangle\Lambda\} \tag{19a}$$

$$f_1(x) = \langle Q_{11}^-(x,\xi)\rangle - 2\pi, \quad f_2(x) = \langle Q_{21}^-(x,\xi)\rangle. \tag{19b}$$

In addition to singularities of the type discussed previously there is an additional problem since $f_2(x) \sim \ln x^2$ as $x \to 0$. This singularity must also be dealt with before numerically solving Eq. 19. The revised form of Eq. 12 requires including a constant term at $x = 0$,

$$\vec{y}(x) = \vec{w}(x) + \Omega(x) \cdot \vec{b} + \vec{c} \quad x < 1 \tag{20a}$$

$$\vec{y}(x) = \vec{w}(x) \quad x > 1 \tag{20b}$$

where, as before, $\vec{w}(x) \to 0$ as $x \to 0$ and $w_1(x) \to 0$ as $x \to \infty$. Arguments similar to those presented in Appendix A show that $c_1 = -1$ and $c_2 = 0$. Then, following the approach described in Appendix B, the analogue to Eq. 14 can be found. For this problem $F(x)$ is

$$F_1(x) = \int_1^\infty d\xi\, Q_{11}^-(x,\xi) - 2\pi + H(x-1)/g \tag{21a}$$

$$F_2(x) = \int_1^\infty d\xi\, Q_{21}^-(x,\xi), \tag{21b}$$

where $H(x-1)$ is a step function; it is 1 if $x < 1$ and 0 if $x > 1$. Formulated in this fashion all singularities have been removed, rapid convergence is assured, and the potential profile can be computed by substituting for $\sigma(\vec{r})$ is the second term of Eq. 2. The integrals in Eq. 21 can be evaluated exactly. The term that contributes to $F_1(x)$

$$\int_1^\infty d\xi\, Q_{11}^-(x,\xi)$$

$$= \frac{4\delta}{S}\left\{\frac{\omega - r}{\omega + 2}\Pi\left(\frac{4}{\omega+2}\backslash\alpha\right) + \frac{\omega + r}{\omega - 2}\Pi\left(\frac{-4}{\omega-2}\backslash\alpha\right)\right\} \tag{22a}$$

$$r = 1 + x, \quad S = \{4\delta^2 + (4 + r)^2\}^{1/2}\omega = 2\{\delta^2 + 1\}^{1/2} \tag{22b}$$

$$\sin\alpha = 2\sqrt{2r}/S \tag{22c}$$

where $\Pi(n\backslash\alpha)$ is the complete elliptic integral of the third kind (Abramowitz and Stegun, 1964); $F_2(x)$ is

$$F_2(x) = G_2(x) - G_2(2\delta - x) \tag{23a}$$

$$G(\gamma) = S[2E(\alpha) - (1 + \cos^2\alpha)K(\alpha)] \tag{23b}$$

$$S = \{9 + \gamma^2\}^{1/2}, \quad \sin\alpha = 2\sqrt{2}/S. \tag{23c}$$

RESULTS AND DISCUSSION

Image Potential

The main result of this paper is the projection method outlined in the preceeding section. It permits accurate and computationally efficient calculation of the electric potential and polarization energy within the model ion pore in response to any electrical source.

Fig. 2 depicts the image potential for an ion at the center of the channel as a function of the half-width to radius ratio, δ, for a model with dielectric constants chosen to mimic a lipid-water system ($\epsilon_1 = 80$, $\epsilon_2 = 2$). The broken line, which is asymptotically exact at large δ, is an approximation suggested by Parsegian:[2] the image potential of an ion at the center of a finite pore is roughly the sum of two terms: that due to an ion in an infinite pore, $\Phi_\infty(K)$, and that due to an ion in the center of a membrane without a pore

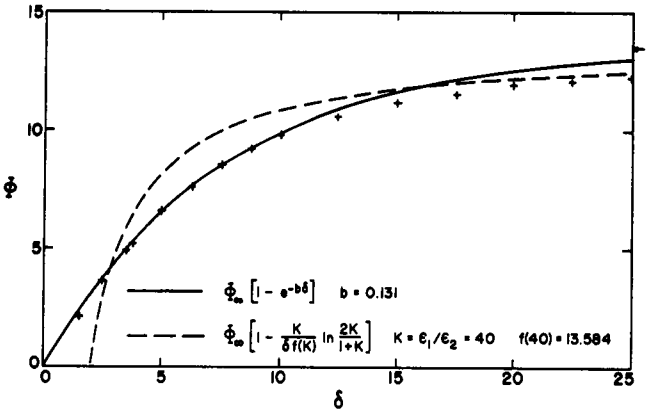

FIGURE 2 Image potential Φ, in units of $e/\epsilon_1 a_0$, for an ion at the center of a cylindrical channel of half-width to radius ratio, δ. The dielectric ratio, ϵ_1/ϵ_2, is 40. In these units, the potential in an infinite channel (denoted by the arrow) is 13.584. The points are calculated using Eq. 14. The broken line is Parsigian's asymptotic approximation, Eq. 24. The solid line is the curve-fitting function, Eq. 25.

$$\Phi(\delta) \approx \Phi_\infty(K) - \frac{K}{\delta}\ln\frac{2K}{K+1}, K \equiv \epsilon_1/\epsilon_2. \tag{24}$$

As δ increases the potential calculated on the basis of Eq. 14 approaches the asymptotic result, which indicates that the method is reliable. Ideally this technique would be tested by carrying out calculations at δ-values large enough that the limiting result, Eq. 24, is found. This is unfortunately not possible since there are still noticeable deviations from the asymptotic slope when $\delta = 40$. In order to carry out a rigorous test, results accurate to better than 0.1% are needed. In this very large δ-domain precise calculations based on Eq. 14 require excessive computer time. By way of comparison, previous calculations, based upon direct numerical analysis of Eq. 4 without prior isolation of the singularities (Levitt, 1978) are only satisfactory for small δ; significant inaccuracies occur when $\delta \gtrsim 6$. The results of the two approaches are contrasted in Table I. As δ increases the importance of treating the singularities exactly becomes quite apparent. For a long, narrow channel ($\delta = 12.5$), previous work underestimates the barrier by $0.83\ e^2/2a_0\epsilon_1$, which, for a univalent ion in a pore of 0.15 nm radius at 300 K, is 1.92 kT; the corresponding estimate of channel conductance would be nearly an order of magnitude too high.

In addition to being more accurate, calculations based upon Eq. 14 require less computational expense. For $\delta = 25$, which is larger than would be found in any system of

[2] As quoted by Levitt (1978).

TABLE I
IMAGE POTENTIAL FOR A MONOVALENT ION IN THE CENTER OF A PORE, AS A FUNCTION OF MEMBRANE HALF-WIDTH, δ.

δ	From Eq. 4*	From Eq. 14
1.5	2.20	2.14
2.5	3.70	3.65
3.5	5.00	4.96
5.	6.56	6.58
6.25	7.60	7.67
8.33	8.74	9.03
8.75	8.91	9.27
12.5	9.83	10.66

Values are in reduced units, $e/\epsilon_1 a_0$; the dielectric ratio, ϵ_1/ϵ_2, is 40.
*As determined from Table I of Levitt (1978).

interest, 70 points along the electrical phase boundaries were needed to obtain 1% accuracy; 0.5% accuracy was achieved using 110 points. In his direct analysis of Eq. 4, Levitt (1978) used 100 points to obtain results which are no longer reliable to within 1% when $\delta > 6$. For such a short pore I find that, using Eq. 14, only 24 points are required to achieve 0.3% accuracy; the 1% level needs just 16 points. Since computational effort is proportional to the square of the number of integration points needed, analysis based upon Eq. 14 appears to cut computational time by roughly 40-fold.

Some further comments should be made about the results presented in Fig. 2. For small δ the maximum in the image potential is well represented by the expression

$$\Phi(\delta) = \Phi_\infty[1 - e^{-b\delta}] \tag{25}$$

where, when $K = 40$, $b = 0.131$. I have found no fundamental justification for this result; it seems to be simply curve fitting. The value of b is chosen to fit data in the intermediate δ range; note that Eq. 25 is not a limiting form, valid as $\delta \to 0$. It is clear that a useful approximation to $\Phi(\delta)$, accurate to within 5% for all values of δ, is given by using Eq. 25 at small to intermediate δ and by using Eq. 24 at large δ. The switchover occurs at δ^* defined such that $\Phi(\delta)$, from Eq. 24, is less than $\Phi(\delta)$, from Eq. 25, for all $\delta > \delta^*$. The same procedure is just as satisfactory with K equal to 10 or 20. In fact, for $K = 10$, 20, and 40, the approximation procedure based on Eqs. 24 and 25 is accurate to within 5% for all δ; in this K range b can be written in terms of a single parameter, $b = 0.826/\sqrt{K}$. Complete curves for large K were not calculated. However, the approximation was tested with $K = 80$ and $66\frac{2}{3}$ for $\delta = 5$, 10, and 15; in each instance the estimate was within 2% of the calculated value. In practice, therefore, the peak in the image potential for a cylindrical pore may be determined using the procedure outlined in this paragraph for any $K \geq 10$. The two necessary parameters are known; $\Phi_\infty(K)$ has been tabulated by Parsegian (1975) and $b(K)$ is given above.

In terms of experimental parameters the peak in the energy barrier for a cylindrical channel is

$$E_{max} = \frac{e^2}{\epsilon d}\Phi(L/d), \tag{26}$$

where d is the channel diameter and L is the membrane width. The energy is clearly much more sensitive to variation of d than of L. For a gramicidinlike channel ($d \sim 0.4$ nm, $L \sim 3$ nm) a 25% increase of d would decrease the barrier by 4.5 kT, corresponding to a 100-fold conductance increase. A 25% decrease in L would lead to a 2.4 kT drop in the barrier, which only increases conductance by a factor of 10. For wide channels like porin (Benz et al. 1978; 1979) the effects are much less important. The diameter is in the range 0.8–1 nm; for such a channel in a 3.0-nm membrane the uncertainty in diameter only leads to a difference of 1 kT in the barrier height estimate or a factor of 3 in conductance.

The Electric Field Due to an Applied Potential

The computational difficulties that caused numerical approximation of Eq. 4 to be unreliable in image potential calculations are even more pronounced in determination of the profile of an applied potential. This is because the inhomogeneous terms in the integral equations for the replacement surface charge density contain singularities near the corner. Numerical analysis of the well-behaved equations generated assuming the functional forms of Eq. 20, yields the results of Fig. 3. Here, the potential profile on the channel axis is plotted as a function of distance from the membrane center for four membrane half-width–to–channel radius ratios, δ. The calculated profiles are substantially different from those found previously (Levitt, 1978).

The electric field well within the pore is constant. The field at the center of the channel and the potential drop across the channel are given in Table II. The results of calculations based upon Eqs. 4 and 20 are contrasted. If

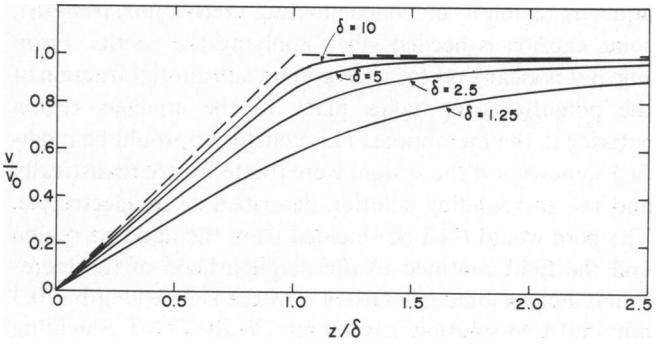

FIGURE 3 Potential profile on the axis of a cylindrical channel as a function of the ratio of the distance from the membrane center to the membrane half-width, z/δ. The broken line represents the pure lipid case. Four membrane half-width–to–pore radius ratios are illustrated. The total potential change across the membrane is $2V_0$.

TABLE II

THE ELECTRIC FIELD AT THE CENTER OF THE CHANNEL AND THE FRACTIONAL POTENTIAL DROP ACROSS THE INTERIOR OF THE PORE AS A FUNCTION OF THE MEMBRANE WIDTH TO PORE RADIUS RATION, δ.

δ	Field at channel center		Fractional potential drop across pore interior	
	From Eq. 20	From Eq. 4*	From Eq. 20	From Eq. 4*
	V_0/δ		V/V_0	
15	0.975		0.950	
10	0.952		0.925	
7.5	0.929		0.901	
5	0.886		0.857	
4.17	0.861	1.08	0.832	0.922
2.5	0.778	1.03	0.744	0.882
1.25	0.625	0.86	0.587	0.735

*Determined from Fig. 3 of Levitt (1978).

Eq. 4 is used, both the electric field and potential drop within the pore are overestimated. As was the case for the peak in the image potential, the data presented in Table II may be summarized empirically

$$\mathcal{E} = \mathcal{E}_0\{1 - e^{-c\sqrt{\delta}}\}, \qquad \delta > 2.5 \tag{27}$$

where $\mathcal{E}$ is the field in the center of the channel and $\mathcal{E}_0$ is the field in the absence of a pore. Again I have no fundamental justification for this result which is accurate to within 1% over the range of δ tested. It should be pointed out that Eq. 27 does not yield accurate estimates of the change in electric field due to the presence of a pore, $(\mathcal{E}_0 - \mathcal{E})/\mathcal{E}_0$, when δ is large; however this quantity is small and of little practical significance. Precise values of the deviation from limiting behavior are not generally necessary. Here too there is also a simple expression for the parameter c which can be used for $10 < K < 80$.

$$1/c = 1.514 - 1.194K^{-1/4}. \tag{28}$$

Because all calculations are carried out assuming the aqueous region to be nonconducting (zero ionic strength), some caution is needed when applying the results. From Fig. 3 it is clear that for wide pores a substantial fraction of the potential drop takes place in the aqueous region exterior to the membrane. This conclusion would be modified somewhat if the system were treated more realistically and the surrounding solution described as an electrolyte. The pore would then be shielded from the aqueous region and the field confined to the neighborhood of the membrane. For an ionic strength of 1 M the Debye length is 0.3 nm; in 0.1 M solution it is 1.0 nm (Wall, 1974). Shielding is essentially complete over 2 Debye lengths.

For a gramicidinlike pore in a 3.0-nm thick membrane δ is ~7.5. From Fig. 3, 10% of the potential drop should take place outside the pore. Shielding does not affect the electric field in this case since < 2% of this drop takes place more than 0.6 nm from the surface. Even 1 M electrolyte cannot substantially affect the potential profile since the electric field is reasonably well confined to the vicinity of the membrane.

For wide pores the situation is different. The δ-value for porin in a 3.0-nm membrane, deduced from conductance and selectivity measurements (Benz et al., 1978; 1979) is in the range of 3–5. This suggests that 15 to 25% of the potential drop could occur outside the pore. In 1 M electrolyte Debye shielding is complete more than ~0.6 nm from the membrane surface; in 0.1 M solution the necessary distance is ~2 nm. If $\delta = 2.5$, 12% of the potential drop takes place more than 0.6 nm into the aqueous region; only 4% occurs more than 2 nm into that region. If $\delta = 5$ the corresponding numbers are 4 and 2%. Thus in 0.1 M electrolytes shielding cannot greatly modify the field profile even with δ as small as 2.5. For 1-M electrolytes there will be substantial alteration of the field profile if $\delta \leq 2.5$ and very little if $\delta \geq 5$. Nonetheless, even with $\delta = 2.5$ and 1 M electrolyte, the electric field is not confined within the pore.

Because the electric field penetrates into the aqueous domain the interpretation of pore conductance data could be affected. Nonohmic current-voltage profiles are often discussed using an Eyring rate theory analysis (Zwolinski et al. 1949). The voltage-dependent contribution to the energy barrier separating two wells in the energy profile is fV_0 where f is the fractional potential change in the particular kinetic step; f is often interpreted as the distance between binding sites divided by the pore length. If the channel is wide or if it only contains a short narrow segment this may be a poor assumption. Refer to Fig. 3 and consider a channel for which 15% of the voltage drop takes place between the solution and an interior binding site. If the pore is narrow ($\delta = 10$), the binding site is ~13% of the distance into the channel. If it is wide ($\delta = 2.5$), the binding site is near the channel mouth. Electrolyte shielding would slightly alter this interpretation for wide channels if the electrolyte concentration is high ($\gtrsim$1 M). The binding site would still be near the channel mouth but somewhat deeper inside than suggested by Fig. 3; the qualitative picture is unaffected.

APPENDIX A

Determination of the Exponent, μ.

The singularities in Y arise from the integrals of Eq. 10. By splitting the integration interval into regions $\xi < x$ and $\xi > x$ and developing $1/(\xi^2 + x^2)$ in power series in (ξ/x) and (x/ξ), respectively, it is easy to show that

$$\int_0^1 \frac{2\xi d\xi}{x^2 + \xi^2}\xi^{-\mu} = \left[\frac{1}{\beta} + 2\beta T(\beta)\right]x^{-\mu} - \frac{1}{\beta} + x^2\varphi(x, \mu) \tag{A1}$$

where $\beta = \mu/2$ and

$$T(\beta) = \sum_{j=1} \frac{(-)^{j-1}}{j^2 - \beta^2} = \sum_{n=0} \beta^{2n} \left\{1 - \frac{1}{2^{2n+1}}\right\} \zeta(2n+2) \quad \text{(A2a)}$$

$$\varphi(x, \mu) = \sum_{j=0} \frac{(-x^2)^j}{j + 1 + \beta} = \int_0^1 \frac{2s\,ds\,s^{\mu}}{1 + x^2 s^2} \cdot \quad \text{(A2b)}$$

Here $\zeta(n)$ is the nth order Riemann Zeta function. From Eqs. 4, 10, and 11 it is then readily seen that, as $x \to 0$,

$$\Omega(x) \cdot \vec{\mathbf{b}} = g\left[\frac{1}{\beta} + 2\beta T(\beta)\right]\Omega(x) \cdot \vec{\mathbf{b}} + 0(1). \quad \text{(A3)}$$

In order that all singularities be contained in $\Omega(x)$, β must be the solution to the equation

$$1 = g\left[\frac{1}{\beta} + 2\beta T(\beta)\right], \quad \text{(A4)}$$

which can be written more conveniently as

$$\mu = 4g \Big/ \left\{1 + \sqrt{1 - 8g^2 T(\mu/2)}\right\} \quad \text{(A5)}$$

and solved by iteration.

APPENDIX B

Construction of the Auxiliary Matrix, $\mathbf{U}(x)$

Combination of Eqs. 4, 11, and 12 permits determination of $\vec{\mathbf{w}}(x)$ and leads immediately to the form Eq. 14. Identification of the auxiliary matrix $\mathbf{U}(x)$ is easy if $x > 1$.

$$\mathbf{U}(x) = \langle \mathbf{Q}(x, \xi) \cdot \Omega(\xi) \rangle, \; x > 1. \quad \text{(B1)}$$

Integration over ξ_1 or ξ_2, denoted by $\langle\ \rangle$, extends between 0 and 1 since $\Omega(\xi)$ is defined in that region only. Identification of $\mathbf{U}(x)$ for $x < 1$ is less obvious. Separating out the ill-defined contributions to Q_{ij}

$$Q^*_{ii}(x, \xi) = Q_{ii}(x, \xi) \qquad i = 1, 2 \quad \text{(B2a)}$$

$$Q^*_{ij}(x, \xi) = Q_{ij}(x, \xi) + 2\xi/(x^2 + \xi^2) \quad i \neq j. \quad \text{(B2b)}$$

$\mathbf{U}(x)$, for $x < 1$, is found to be

$$\mathbf{U}(x) = \langle \mathbf{Q}^*(x, \xi) \cdot \Omega(\xi) \rangle + \langle \mathbf{S}(x, \xi) \cdot \Omega(\xi) \rangle - \frac{1}{g}\Omega(x) \quad \text{(B3a)}$$

$$S_{11} = S_{22} = 0, \qquad S_{12} = S_{21} = -2\xi/(x^2 + \xi^2). \quad \text{(B3b)}$$

Employing the analysis of Appendix A to project out the singularity leads ultimately to the result,

$$\mathbf{U}(x) = \langle \mathbf{Q}^*(x, \xi) \cdot \Omega(\xi) \rangle - \mathbf{I}/\beta - \mathbf{\Gamma}(x), \qquad x < 1 \quad \text{(B4a)}$$

$$\Gamma_{11} = \Gamma_{22} = -x^2 \int_0^1 \frac{dt\, S(\sqrt{t})}{1 + x^2 t},$$

$$\Gamma_{12} = \Gamma_{21} = x^2 \int_0^1 \frac{dt\, C(\sqrt{t})}{1 + x^2 t} \quad \text{(B4b)}$$

with C and S defined by Eq. 11b.

APPENDIX C

Modification of the Method of Averaging Functional Corrections

The method of averaging functional corrections (Luchka, 1965) is a modified successive-approximations approach to integral equations that both enlarges the region of convergence and reduces the number of iterations required to achieve the desired numerical accuracy. For simultaneous equations of the form

$$\vec{\mathbf{w}}(x) = g[\mathbf{F}(x) + \langle \mathbf{Q}(x, \xi) \cdot \vec{\mathbf{w}}(\xi) \rangle] \quad \text{(C1)}$$

the nth iterative correction to the solution incorporates a term of the form

$$\langle \mathbf{Q}(x, \xi) \rangle \cdot \vec{\alpha}_n \quad \text{(C2)}$$

where α_n is the mean value of the correction. Since the electrostatic kernel functions, as discussed previously, propagate singularities unless care is taken, this method of approximation must be modified if it is to be of use here.

Successive corrections to $\vec{\mathbf{w}}(x)$ and $\vec{\mathbf{b}}$, $\vec{\delta}_n(x)$ and $\vec{\mathbf{d}}_n$, respectively, are defined as

$$\vec{\mathbf{w}}(x) \equiv \sum_{n=0} \vec{\delta}_n(x), \vec{\mathbf{b}} \equiv \sum_{n=0} \vec{\mathbf{d}}_n. \quad \text{(C3)}$$

Since $\vec{\mathbf{w}}(x)$ and therefore the $\delta_n(x)$ are $0(x^{1-\mu})$ as $x \to 0$, a weighting function

$$V(\xi) = \xi^{1-\mu}/(1 + \xi^{1-\mu}) \quad \text{(C4)}$$

is introduced to suppress integration singularities in Eq. C2; $V(\xi)$ behaves like $\vec{\mathbf{w}}(\xi)$ for small ξ and approaches 1 when ξ is large. Finally the integration over ξ_1 is truncated so that it is of finite range, $0 \leq \xi_1 \leq R^*$. It is now possible to formulate a convergent iterative solution to Eq. 14, which incorporates functional corrections. The zeroth approximation is

$$\vec{\mathbf{d}}_0 = \mathbf{R} \cdot \vec{\mathbf{F}}(0), \qquad \vec{\delta}_0(x) = g[\vec{\mathbf{F}}(x) + \mathbf{U}(x) \cdot \vec{\mathbf{d}}_0], \qquad \mathbf{R} \cdot \mathbf{U}(0) = -1. \quad \text{(C5)}$$

Defining $\vec{\alpha}_0 \equiv 0$, the successive corrections are

$$\vec{\delta}_n(x) = g[\langle \mathbf{Q}(x, \xi) \cdot \{\vec{\delta}_{n-1}(\xi) + V(\xi)(\vec{\alpha}_n - \vec{\alpha}_{n-1})\}\rangle + \mathbf{U}(x) \cdot \vec{\mathbf{d}}_n] \quad \text{(C6a)}$$

$$\vec{\mathbf{d}}_n = \mathbf{R} \cdot [\langle \mathbf{Q}(0, \xi) \cdot \{\vec{\delta}_{n-1}(\xi) + V(\xi)(\vec{\alpha}_n - \vec{\alpha}_{n-1})\}\rangle] \quad \text{(C6b)}$$

$$\vec{\alpha}_n = g\mathbf{Z} \cdot \mathbf{M} \cdot [\langle \{\overline{\mathbf{Q}(x, \xi)} + \mathbf{W} \cdot \mathbf{Q}(0, \xi)\} \cdot \vec{\delta}_{n-1}(\xi)\rangle - \mathbf{S} \cdot \vec{\alpha}_{n-1}] \quad \text{(C6c)}$$

where α_n is the average value of $\alpha_n(x)$, the bar indicates integration over the variables x_1 or x_2 and

$$\mathbf{M} = \begin{pmatrix} 1/R^* & 0 \\ 0 & 1/\delta \end{pmatrix}, \qquad \mathbf{W} = \overline{\mathbf{U}(x)} \cdot \mathbf{R} \quad \text{(C7a)}$$

$$\mathbf{Z} = (1 - g\mathbf{M} \cdot \mathbf{S})^{-1}, \qquad \mathbf{S} = \langle \{\overline{\mathbf{Q}(x, \xi)} + \mathbf{W} \cdot \mathbf{Q}(0, \xi)\} V(\xi) \rangle. \quad \text{(C7b)}$$

This research was partially supported by grant number GM-28643 from the National Institutes of Health. I wish to thank Professor Peter Läuger for interesting me in this problem.

Received for publication 30 November 1981 and in revised form 22 March 1982.

REFERENCES

Abramowitz, M., and I. A. Stegun, editors. 1965. Handbook of Mathematical Functions. Dover Publications, Inc., New York. 589–626.

Benz, R., K. Janko, W. Boos, and P. Läuger. 1978. Formation of large, ion-permeable membrane channels by the matrix protein (porin) of *Escherichia coli*. *Biochim. Biophys. Acta.* 511:305–319.

Benz, R., K. Janko, and P. Läuger. 1979. Ionic selectivity of pores formed by the matrix protein (porin) of *Escherichia coli*. *Biochim. Biophys. Acta.* 551:238–247.

Erdogan, F., and G. D. Gupta. 1972. On the numerical solution of singular integral equations. *Quart. Appl. Math.* 29:525–534.

Jordan, P. C. 1981. Energy barriers for the passage of ions through channels. Exact solution of two electrostatic problems. *Biophys. Chem.* 13:203–212.

Levitt, D. G. 1978. Electrostatic calculations for an ion channel. I. Energy and potential profiles and interactions between ions. *Biophys. J.* 22:209–219.

Luchka, Y. A. 1965. The Method of Averaging Functional Corrections. Theory and Applications. Academic Press, Inc. New York 34–52.

Parsegian, V. A. 1969. Energy of an ion crossing a low dielectric membrane: solutions to four relevant electrostatic problems *Nature (Lond.)*. 221:844–846.

Parsegian, V. A. 1975. Ion-membrane interactions as structural forces. *Ann. N. Y. Acad. Sci.* 264:161–174.

Urry, D. W. 1971. The gramicidin A transmembrane channel:a proposed $\pi_{(L,D)}$ helix. *Proc. Natl. Acad. Sci. U. S. A.* 68:672–676.

Wall, F. T. 1974. Chemical Thermodynamics. 3rd edition W. H. Freeman and Co., San Francisco 433–439.

Zwolinski, B. J., H. Eyring, and C. E. Reese, 1949. Diffusion and membrane permeability. *J. Phys. Chem.* 53:1426–1453.